Phase Continuity in High Temperature Mo-Si-B Alloys: A FIB-Tomography Study

O. Hassomeris[1], G. Schumacher[1,a], M. Krüger[2], M. Heilmaier[3], J. Banhart[1]

[1]*Helmholtz-Zentrum Berlin für Materialien und Energie GmbH, Hahn-Meitner-Platz 1, D-14109 Berlin, Germany*
Otto-von-Guericke Universität Magdeburg, Institute for Materials and Joining Technology, Große Steinernetischstraße 6, D-39104 Magdeburg, Germany
[3]*TU Darmstadt, Materials Science (FB 11), Petersenstr. 23, D-64287 Darmstadt, Germany*

The microstructure of mechanically alloyed Mo-Si-B materials of different compositions has been studied by X-ray diffraction and FIB-tomography. Three different phases were found in all alloys: α-Mo solid solution, T2-phase (Mo_5SiB_2-type) and A15-phase (Mo_3Si). The Mo-6Si-5B and Mo-9Si-8B (at%) alloys reveal a continuous morphology of the α-Mo phase. In Mo-9Si-8B the α-Mo phase is distributed more homogeneously compared to the Mo-6Si-5B alloy. In contrast, Mo-13Si-12B does not possess a continuous α-Mo-phase. The consequences for the mechanical properties and oxidation resistance are discussed.

[a]Corresponding author: Gerhard Schumacher, e-mail address: Schumacher@helmholtz-berlin.de

1. Introduction

The use of Ni-base superalloys in stationary and aircraft turbines is restricted to temperatures below about 1150 °C [1]. The design of structural materials with service temperatures well above that of nickel-base superalloys requires the melting point of these new structural materials to exceed appreciably that of nickel base superalloys. Moreover, the oxidation resistance and fracture toughness must be sufficiently high. Mo-Si-B alloys are promising candidates for many of such high temperature applications [2]. Berczik [3,4] established Mo-Si-B alloys containing a α-Mo solid solution phase, Mo_5SiB_2 phase (known as T2 phase) and Mo_3Si phase. The T2-phase is tetragonal, while Mo_3Si exhibits the cubic A15 structure. The α-Mo phase is known to be fairly ductile while both T2 and A15 phases are brittle [1]. The T2 phase reveals reasonable oxidation resistance [5]. Thus, at temperatures above 1000°C the diffusion of Si and B to the surface is decisive for the formation of a dense, protective borosilicate glass surface layer which limits the diffusion pathways of oxygen from the surface into the bulk [6]. The distances between the T2-precipitates should therefore be sufficiently small to allow for the creation of a continuous borosilicate glass surface layer.

Mo-Si-B alloys having potential as ultra-high-temperature structural materials can be designed with microstructures containing either individual α-Mo particles or a continuous α-Mo phase [7]. On the one hand, for good oxidation resistance, a discontinuous α-Mo phase is more appropriate to avoid extensive mass loss by formation of MoO_3 [6]. Assuming a two phase system where individual α-Mo particles are embedded in a continuous Mo_5SiB_2 matrix phase provides reasonable oxidation resistance but poor ductility. In the second case, the continuous α-Mo phase ensures a higher ductility and fracture toughness, but the oxidation

resistance is expected to be poor. Hence, the various requirements are in conflict with each other. On the other hand, if the spacing between the individual Mo_5SiB_2 particles decreases down to the scale of dislocation pile-ups due to a reduction of the volume fraction of the α-Mo phase, the mechanical properties are expected to change [8]. Both the oxidation resistance and the mechanical properties thus depend sensitively on the microstructure of the alloy [9] which is determined by the composition and the processing mode.

Two-dimensional analysis cannot provide reliable information about phase distribution and contiguity. We therefore studied the microstructure of three Mo-Si-B alloys of different composition by focused ion beam (FIB) - tomography. In combination with appropriate visualization software this technique allows obtaining 3-dimensional information about the microstructure of the material with sufficiently high resolution of less than 20 nm [10].

2. Experimental

Three alloys of different compositions (Mo-6Si-5B, Mo-9Si-8B and Mo13-Si-12B in at%) were produced by powder metallurgy. The elemental powders were milled in a planetary ball-mill for 20 h with 200 rpm in order to achieve a homogeneous distribution of elements as well as the formation of a Mo-Si-B solid solution (a more detailed description of the mechanical alloying process of Mo-Si-B alloys is given in [11]). Afterwards, the material was isostatically pressed at room temperature in order to increase the mass density and to decrease the number of pores. During the subsequent pressure-less sintering process the material was consolidated at 1600°C. Residual pores were closed during subsequent hot isostatic pressing at 1500°C and 200 MPa in order to increase the mass density and to improve the mechanical properties. Residual porosity was measured to be below 1% [11].

Cubes were cut out of the alloys and subsequently ground and polished. In order to obtain a good contrast for a scanning electron microscope (SEM) each surface was etched in Murakami's reagent resulting in the removal of the T2- and A15- phases [12, 13]. The etched specimens were then fixed with conductive silver on a holder and transferred into the SEM.

Tomographic data sets were obtained in a focused ion beam (FIB, Zeiss 1540 Crossbeam) by serial sectioning. The material was removed with a Ga-ion beam. The optimum beam current and voltage of the Ga-beam were 500 pA and 30 kV, respectively, while the cutting depth was 70 μm. Use of these parameters prevented the occurrence of the curtaining effect, i.e., the irregular removal of material. The SEM micrographs were recorded using a voltage of 5 kV. A secondary electron (SE) - detector or an energy and angle selective backscatter electron (EsB) – detector were used to scan the surface of etched and un-etched specimens, respectively. More than 200 sections were recorded for each tomogram. In order to correct the drift of the micrograph during the recording of the tomogram, we used a pore on the top surface of the specimen as a marker to shift each micrograph to the correct position (see Fig. 1). The shift of the electron beam in lateral direction due to slice cutting during recording of the tomogram (see Fig. 1) was calculated and subsequently corrected with the program "Image J". Boolean images were then created by the use of appropriate ranges for the gray values which were 0-159 and 160-155 to determine the volume fraction of T2+A15 phases and α-Mo, respectively. Some measurements performed on Mo-13Si-12B were carried out utilizing a different detector. In this case the corresponding gray values were 0-50 and 100-255 for the T2 and A15 phases and the α-Mo phase, respectively. The figures were further processed with the software program "VG-Studiomax". Sectioning of the volume allows for the display of the individual phases and the determination of their volume fractions. From the series of SEM micrographs, a 3-dimensional representation of the investigated volume was generated by interpolation, also by "VG-Studiomax". The results were verified by the

software program "Avizo". This program uses the "labelling by reconstruction" technique, based on the "neighbourhood-algorithm" [14]. This algorithm comprises neighbouring voxels with the same gray scale to local objects. Non-continuous ranges were identified and marked by colours.

X-ray diffraction spectra were recorded in a Bruker D8 diffractometer using Cu Kα radiation. The measured spectra were analysed with the software program "EVA".

3. Results

Figs. 2a-c show XRD spectra of the non-etched alloys Mo-6Si-5B, Mo-9Si-8B and Mo-13Si-12B. All three alloys reveal Bragg reflections that can be assigned to one of the three phases, α-Mo, T2-phase or A-15-phase. The different intensities of the Bragg-reflections for the different alloys are in qualitative agreement with the volume fractions of the phases expected from the alloy compositions.

The XRD spectra of the alloys Mo-6Si-5B, Mo-9Si-8B and Mo-13Si-12B after etching with Murakami's reagent are depicted in Figs. 2d-f. In Mo-6Si-5B and Mo-9Si-8B, only the reflections of the α-Mo phase are visible while in the Mo-13Si-12B alloy the Bragg-reflections of all three phases α-Mo, T2-phase and A15-phase are present. The intensities of the reflections belonging to the A15- and T2- phase after etching are smaller than the corresponding intensities of the non-etched specimen. Obviously, both the T2- and the A15-phases have been totally removed from the surface of Mo-6Si-5B and Mo-9Si-8B alloy by etching on a depth scale of several μm. In the Mo-13Si-12B alloy, the T2- and A15- phases have been etched until saturation of the etching solution was reached, resulting in individual α-Mo-rich areas that protrude above the surface and the surrounding matrix consisting of mainly T2- and A15-phases (see Fig. 3).

The reconstructed volume of the α-Mo-phase in the etched Mo-6Si-5B alloy is shown in Fig. 4a. The analysis of the subsequent sections of the tomogram yields a continuous α-phase. The A15- and T2-phases have both been dissolved during etching and can therefore not be distinguished in the tomogram. In the following, they will be denoted as "T2+A15" phase. Together they have a largely continuous morphology (see Fig. 4b). The volume fractions of the phases are listed in Table 1. The distribution of the phases in Mo-6Si-5B alloy seems to be heterogeneous in the small volume element investigated by FIB tomography.

Compared to the Mo-6Si-5B alloy, the distribution of phases in the Mo-9Si-8B alloy is more homogeneous (see Fig. 5a). Both α-Mo and T2+A15 phases are continuous as can be seen from Fig. 5b. The volume fractions of the α-Mo and the T2+A15 phases are nearly identical (see Table 1).

The reconstructed volume of the α-Mo phase recorded in the Mo-poor areas of Mo-13Si-12B alloy (see Fig. 3) is shown in Fig. 6a. A detailed analysis of the cut segments of Fig. 6a reveals a discontinuous α-Mo-phase. The phase distribution of α-Mo is rather heterogeneous and the size varies strongly from particle to particle, see Fig. 6b.

Fig. 7 reveals the reconstructed volume of the etched Mo-13Si-12B alloy recorded in the Mo-rich area of Fig. 3. In this area the volume fraction of the α-Mo phase is 89 vol. %. This value is even larger than the mean values measured in the Mo-6Si-5B and Mo-9Si-8B alloys (see Table 1). Furthermore, within the analysed volume the distribution of the T2+A15 phase is heterogeneous (see Fig. 7b).

3

4. Discussion

A comparison of the three alloys shows that the volume fraction of α-Mo decreases with increasing content of Si and B (see Table 1). The volume fractions of α-Mo in the Mo-9Si-8B and Mo-6Si-5B alloy agree well with the values based on SEM investigations reported by Heilmaier et al. [15] for alloys of the same composition. Because of the heterogeneous microstructure of alloy Mo-13Si-12B the values of the volume fraction of α−Mo depend on the area where the tomography has been recorded. The volume fraction of α-Mo obtained from the measurements in the Mo−rich areas is high (89%) while the value determined in the surrounding matrix is low (14%). Taking into account the volume fraction of the Mo−rich area (~ 5%) determined by analysis of the areas of the phases leads to a mean volume fraction of α-Mo of 17%. This value is appreciably smaller than the value of 30% reported by Heilmaier et al. [15]. This discrepancy might lie in the heterogeneity of the alloy which could be caused by insufficient homogenization of the powder particles after 20 hours of milling. The specimen volumes analysed in this work are sufficiently large to provide representative values for the whole specimen if the material is homogeneous, but are too small to provide an average value if the material is heterogeneous as it is the case for the Mo-13Si-12B alloy.

A nearly homogeneous phase distribution could only be detected in the Mo-9Si-8B alloy. At low Si and B content the α-Mo phase dominates the microstructure while at high Si and B content the T2+A15 phases are dominant. The Mo-13Si-12B alloy shows non-continuous α-Mo in some parts of the sample. The α-particles are distributed inhomogeneously and are very different from each other in size and morphology.

An alloy with non-continuous microstructure similar to that of Mo-13Si-12B was reported by Schneibel et al. [9]. In that alloy, α-Mo particles of 21 vol. % are embedded in a T2+A15 matrix. A low fracture toughness of 4.1 MPa m$^{1/2}$ was reported [8] for that alloy in agreement with predictions derived from the microstructure. In the reconstructed tomogram of our alloy non-continuous areas of α-Mo with a volume fraction of 14% embedded in a T2+A15 matrix are visible. We therefore also expect a low fracture toughness for our Mo-13Si-12B alloy. For continuous α-Mo with 40% volume fraction a distinct increase in fracture toughness compared to the alloy with 21% α-Mo phase has been found [8]. An even higher fracture toughness can be expected for the Mo-6Si-5B and Mo-9Si-8B alloy in which the volume fraction of α-Mo is even larger than 50% (see Table 1).

Both monolithic phases Mo$_3$Si and Mo$_5$SiB$_2$ were shown to reveal high creep resistance at elevated temperatures [16,17] The creep resistance of Mo-Si-B multiphase alloys depends sensitively on the microstructure and on the volume fraction of the α-Mo phase [6,9]. A small volume fraction (21%) of the non-continuous α-Mo phase yields a high creep resistance [6]. The presence of a continuous α-Mo phase would lower the creep resistance of the material, as one might suppose that the T2 and A15 phase would play a minor role in the deformation of the composite material due to the presence of a deformable α-Mo phase [6]. A non-continuous α-Mo phase was detected for a Mo-13Si-12B alloy. Therefore, a high creep resistance can be expected for this alloy. Contrary to Mo-13Si-12B, the continuous α-Mo-phase found in alloys Mo-6Si-5B and Mo-9Si-8B points to a reduced creep resistance though their creep resistance was found to be still superior to the current state of the art nickel-base single crystal superalloy CMSX 4 [18].

For a high oxidation resistance a small volume fraction of α-Mo is advantageous. This is due to the fact that α-Mo forms a volatile oxide (MoO$_3$) [6]. A continuous α-Mo-phase would therefore cause a larger loss of mass, while for a non-continuous α-phase the mass loss would be smaller, as particles far from the surface are shielded by the surrounding T2+A15 matrix. The T2 phase forms a B$_2$O$_3$ layer on the surface which acts as a diffusion barrier for oxygen,

and therefore prevents further oxidation [6]. For the Mo-6Si-5B and Mo-9Si-8B alloys, a smaller oxidation resistance can therefore be expected due to the high volume fraction of the α-phase. However, recent results on a composition of Mo-9Si-8B with several microalloying additions such as for instance Zr show encouraging results [19]: due to the fineness of the microstructure the Mo loss can be controlled and remains on a very low level.

Unlike the alloys Mo-6Si-5B and Mo-9Si-8B, the microstructure of the Mo-13Si-12B alloy consists of small α-Mo precipitates embedded in the T2+A15 matrix. This microstructure suggests that the oxidation resistance of this alloy is relatively high.

5. Summary and Conclusions

The microstructure of three Mo-Si-B alloys has been examined by X-ray diffraction and FIB-tomography using the serial sectioning technique. The continuity of the α-Mo-phase and of the T2 + A15 phases has been determined by 3-dimensional analysis of the FIB-tomograms. The α-phase and the volumes containing both the T2 + A15 phases were found to be continuous in both the alloys Mo-6Si-5B and Mo-9Si-8B while in the Mo-13Si-12B the α-Mo-phase is not continuous. Furthermore, in the latter alloy the microstructure was found to be heterogeneous. As a consequence, the volume fractions of the α-phase (and of the complementary combined T2 + A15 phases) measured in different areas of the Mo-13Si-12B alloy differed appreciably. An optimum compromise between high temperature creep and oxidation resistance as well as ambient temperature toughness, thus, requires a judicious balance between microstructural scale, volume fraction and contiguity of the Mo solid solution phase.

References

[1] Dimiduk DM, Perepezko JH. MRS Bulletin 2003;September:639.

[2] Schneibel JH. *"Beyond Nickel-Base Superalloys",* Oak Ridge: Oak Ridge National Laboratory, 2001. TN 37831-6115; Proc. Thirteenth Int. Conf. Processing and Fabrication of advanced Materials (PFAM XIII) Singapore, Dec. 6-8 (2004).

[3] Berczik DM. *"Method for enhancing the oxidation resistance of a molybdenum alloy, and a method of making a molybdenum alloy". 5,595,616* United States Patent, 1997.

[4] Berczik DM. *"Oxidation Resistant Molybdenum Alloys." 5,693,156* United States Patent, 1997.

[5] Ito K, Hayashi T, Yokobayashi M, Murakami T, Numaraka H. Metall Mater Trans 2005;36A:627

[6] Schneibel JH, Ritchie RO, Kruzic JJ, and P. F. Tortorelli, Metall Mater Trans 2005;36A:525.

[7] Schneibel JH, Kramer MJ, Easton DS., Scripta Mater 2001;46:217.

[8] Mendiratta MG, Parthasarathy TA, Dimiduka DM. Intermetallics 2002;10:225.

[9] Schneibel JH, Kruzic JJ, Ritchie RO. "*Mo-Si-B Alloy Development*". Oak Ridge: Proceedings of the 17th Annual Conference on Fossil Energy Materials (2003).

[10] Holzer L, Indutnyi F, Gassser PH, Münch B, Wegmann M. J. Microsc. 2004;216:84.

[11] Krüger M, Franz S, Saage H, Heilmaier M, Schneibel JH, Jéhanno P, Böning M, Kestler H, Intermetallics 2008;16:933.

[12] Meyer MK, Kramer MJ, Akinca M. Intermetallics 1996;4:273.

[13] Schneibel JH, Liu CT, Easton DS, Carmichael CA, Mater Sci Eng 1999:A261:78.

[14] Armbrecht J, Sych T, Robb K. "MAVI - Modular Algorithms for Volume Images V1.2.1". s.l. : Fraunhofer Institut für Techno- und Wirtschaftsmathematik, 2006. Kapitel 1: pp. 2.

[15] Heilmaier M, Saage H, Krüger M, Jehanno P, Böning M, Kestler H, Drawin S. JSPS Report of the 123rd Committee on Heat Resisting Materials and Alloys 2007:;48:245.

[16] Rosales I, Schneibel JH, Heatherly L, Horton JA, Martinez L, Campillo B. Scripta Mater 2003;48:185.

[17] Ihara K, Itoh K, Tanaka K, Yamaguchi M. Mater Sci Eng 2002;A329:222.

[18] Heilmaier M, Krüger M, Saage H, Rösler J, Mukherji D, Glatzel U, Völkl R, Hüttner R, Eggeler G, Somsen C, Depka T, Christ H-J, Gorr B, Burk S, JOM 2009;61:61.

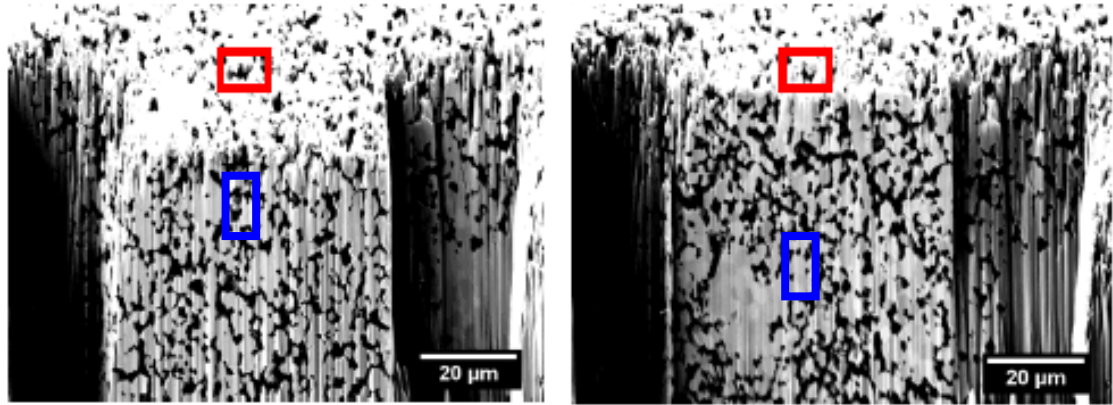[19] Burk S, Gorr B, Trindade VB, Krupp U, Christ HJ. Corr Eng Sci Tech 2009;44:168.

Fig. 1: SEM of Mo-6Si-5B alloy recorded after the first (a) and last (b) cut of the tomogram of the Mo-6Si-5B alloy.
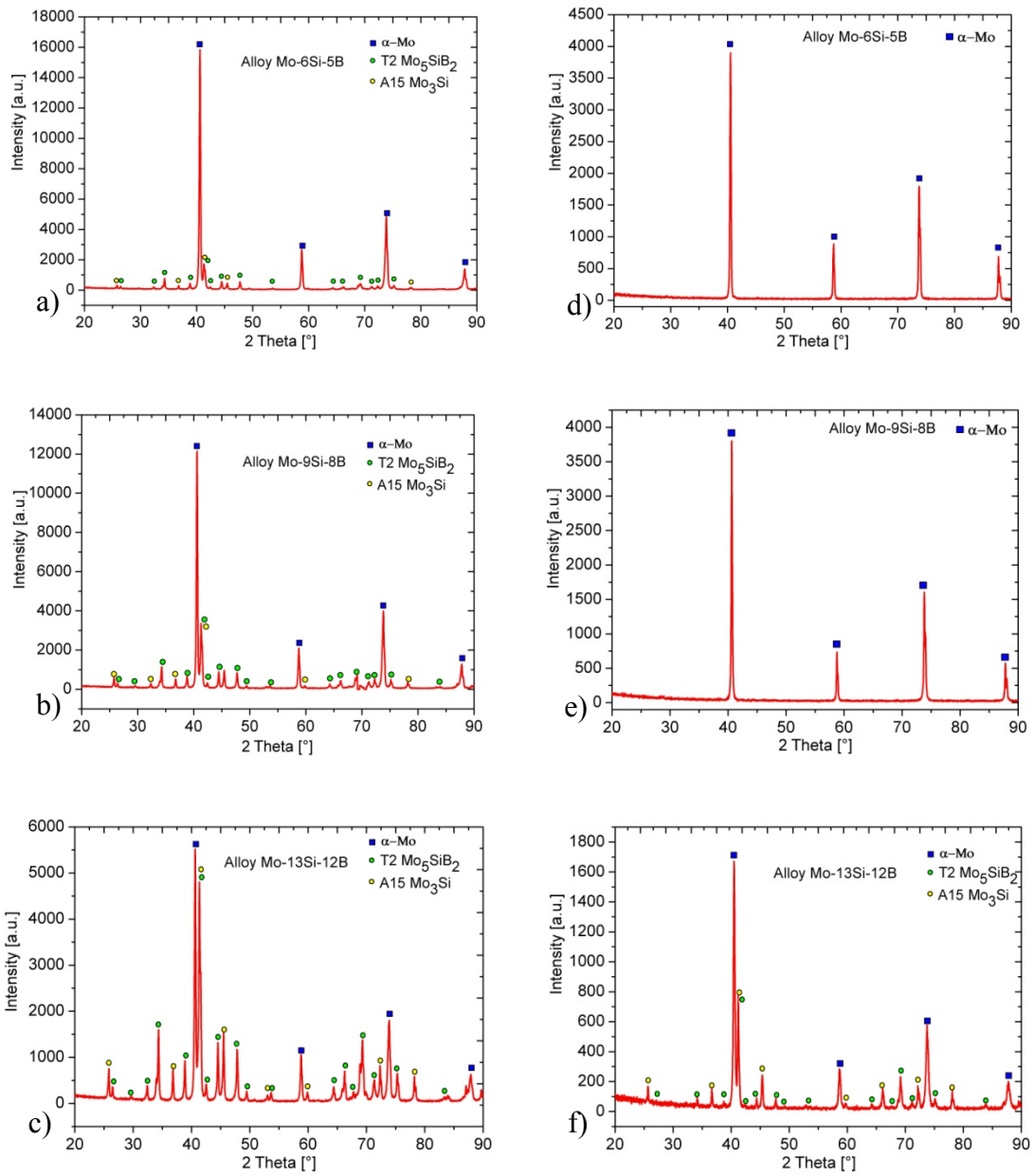
Fig. 2: XRD spectra of Mo-6Si-5B (top), Mo-9Si-8B(middle) and Mo-13Si-12B(bottom) alloy in the as-polished condition (a-c) and after etching with Murakami's solution (d-f).
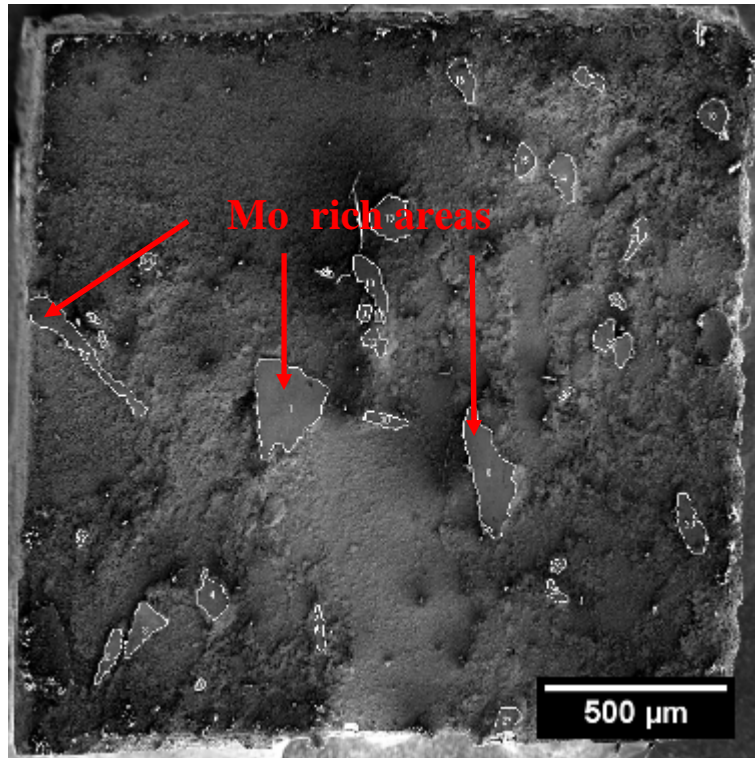
Fig. 3: Micrograph of the Mo-13Si-12B alloy after etching with Murakami's reagent. The marked areas are α-Mo-rich areas that were hardly etched by the Murakami's reagent.
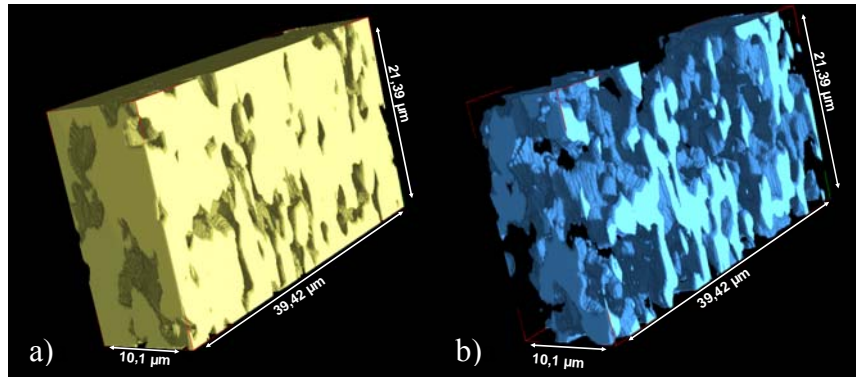
Fig. 4: Reconstructed volume of the α-Mo-phase (a) and of the complementary T2 + A15-phases (b) in the Mo-6Si-5B alloy. The yellow range in (a) denotes the surface. The dark ranges are caused by shadow effects and show the α-Mo-phase. The T2 + A15 phase is coloured dark blue while its surface is light blue.
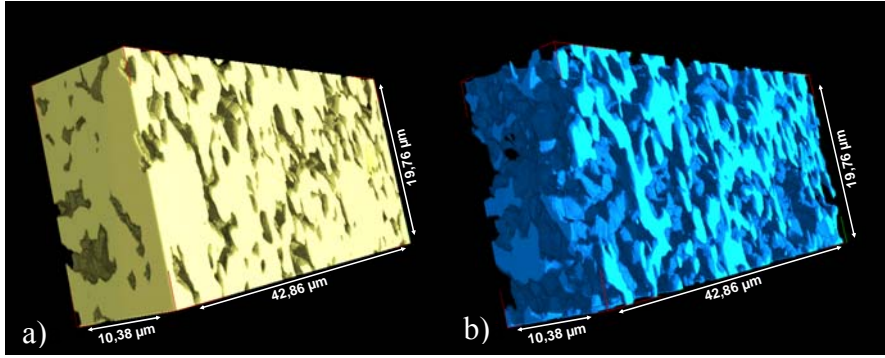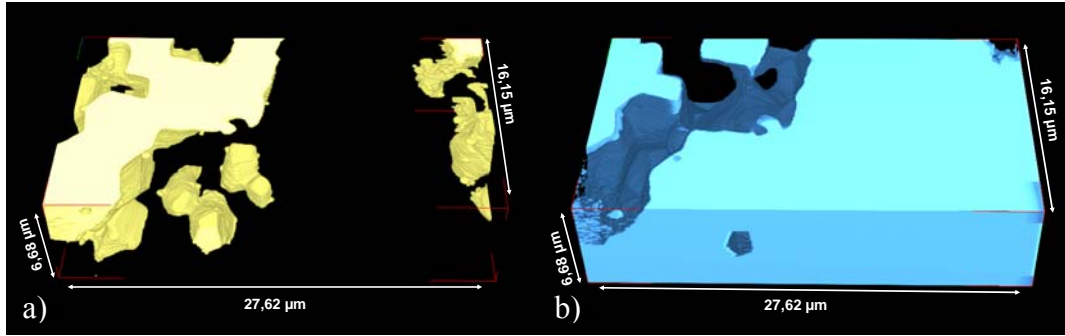
Fig. 5: Same as Fig. 4 for Mo-9Si-8B alloy.

Fig. 6: Reconstructed volume of the α-Mo-phase (a) and of the complementary T2+A15-phases (b) of the Mo-13Si-12B alloy. The yellow range in (a) denotes the α-phase, the surface is indicated by bright yellow colour. The T2+A15 phases in (b) are indicated by dark blue colour while their surface is light blue.
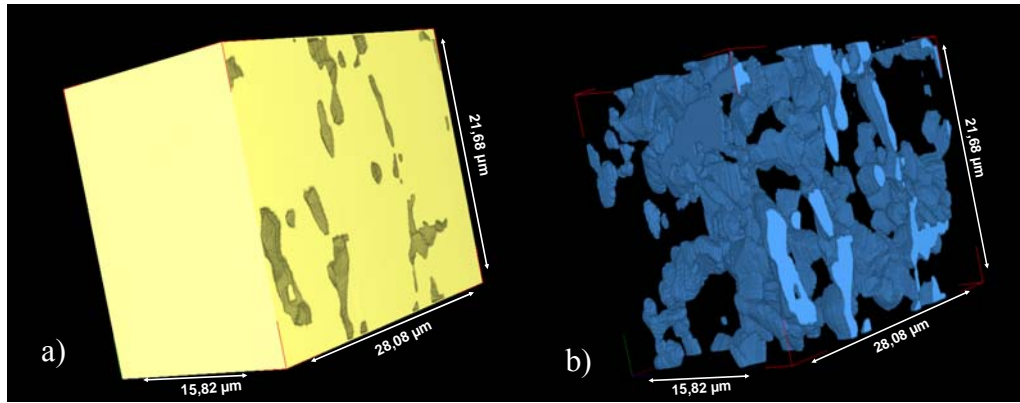
Fig. 7: Reconstructed volume of the Mo-rich area of the Mo-13Si-12B alloy marked in Fig. 3. The α-Mo-phase is depicted in yellow colour (a) while the T2+A15-phases in (b) are dark blue. The surface of T2+A15 is displayed in light blue.

Table 1. Total volume and volume fractions of α-Mo and T2+A15 phases determined in this work and given by Heilmaier et al (Ref. 15)

alloy	Total volume (μm^3)	α-Mo (μm^3)	T2+A15 (μm^3)	α-Mo (%)	T2+A15 (%)
Mo-6Si-5B	8517	6224	2229	73 (this work)	27
Mo-6Si-5B				70 (Ref. 14)	
Mo-9Si-8B	8792	4914	3878	56 (this work)	44
Mo-9Si-8B				55 (Ref. 14)	
Mo-13Si-12B In matrix, Fig. 2	2988	406	2582	14 (this work)	86
Mo-13Si-12B In Mo-rich areas at Fig. 4	9636	8599	1037	89 (this work)	11
Mo-13Si-12B				30 (Ref. 14)	